energy&fuels

pubs.acs.org/EF

Article

Fluidized Bed Pyrolysis of Biomass: A Model-Based Assessment of the Relevance of Heterogeneous Secondary Reactions and Char Loading

Maurizio Troiano, Valeria Ianzito, Roberto Solimene, Elvis Tinashe Ganda, and Piero Salatino*

Cite This: *Energy Fuels* 2022, 36, 9660−9671

Read Online

ACCESS | Metrics & More | Article Recommendations

ABSTRACT: A model of non-catalytic fast fluidized bed pyrolysis of biomass has been developed with the aim of investigating the relevance of secondary heterogeneous reactions between primary products of biomass decomposition and the char accumulated in the bed. The fate of biomass and the extent of biomass and char holdup in the pyrolyzer have been modeled by considering entrainment and elutriation of biomass and char particles, char attrition, as well as bed drain/regeneration. The kinetics of primary and secondary pyrolitic reactions is modeled according to a semi-lumped reaction network using kinetic parameters selected among published correlations. The rate of heterogeneous volatile−char secondary reactions has been modeled borrowing a kinetic expression from the neighboring area of tar adsorption/decomposition over char during biomass gasification. Model computations are helpful to assess the role of heterogeneous vapor−char secondary reactions. The sensitivity of the pyrolyzer performance on char loading in the bed as a result of combined char entrainment, elutriation, attrition, and bed drain/regeneration, the extent of gas-phase backmixing, the process temperature, the gas superficial velocity and residence time, and the particle size is demonstrated and discussed. Model results provide useful guidelines and pinpoint future research priorities for optimal design and control of fluidized bed pyrolyzers.

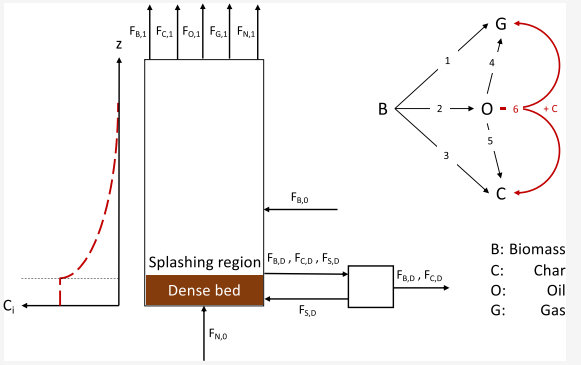

1. INTRODUCTION

The biomass-pyrolysis-based technology platform has the potential to give a major contribution to decarbonization by supporting the shift from the current oil refinery infrastructure to a biorefinery-based production of sustainable chemicals and fuels. Fast pyrolysis offers a direct route for the production of liquid fuels and chemicals from residual, low indirect land-use change (ILUC) biomass, with remarkable feedstock flexibility and energy input efficiency compared to alternative thermochemical pathways. Fast pyrolysis has the potential of converting all carbon in the feedstock unlike biological processes, which can only valorize the non-recalcitrant fraction of biomass.[1,2] The need for large economies of scale required for biomass biorefinery to compete with fossil fuels encourages an extended supply chain and distributed system approach to biomass valorization based on decentralized processing of raw feedstock and generation of biogenic intermediates (biofeedstocks) at satellite biomass harvesting/collection sites, which then feed into larger centralized processing or upgrading biorefineries.[3] For this to be economical, processes and reactors for mass production of biogenic intermediates and end products need to be reengineered.

Fast pyrolysis generates solid (biochar), liquid (bio-oil), and gases through a complex chemical network of series−parallel thermally activated reactions starting with depolymerization of lignocellulosic biopolymers (cellulose, hemicellulose, and lignin), followed by fragmentation, rearrangement/isomerization, repolymerization, aromatization, volatilization, and condensation reactions.[4−7] The inherent heterogeneity of biomass raw feedstocks and the complexity of chemical pathways are responsible for the broad variety of chemical compounds in the bio-oil, including pyrolytic sugars and oligosaccharides, furans, alkylphenols, acids, ketones, and aldehydes, together with substantial amounts of water. The complex composition and some problematic properties (high viscosity, acidic pH, low heating value, and limited stability) of bio-oils may jeopardize their further processing and use.[8] These potential drawbacks are driving research toward the improved design of pyrolytic converters and choice of process conditions that may maximize yield and selectivity toward valuable compounds. Catalytic pyrolysis,[9−12] fractional/staged

Special Issue: 2022 Pioneers in Energy Research: Anders Lyngfelt

Received: May 8, 2022
Revised: July 10, 2022
Published: August 18, 2022

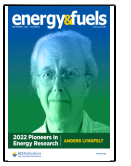

pyrolysis,[13,14] and co-pyrolysis with non-recyclable plastics[15] represent some of the variants of basic isothermal non-catalytic fast pyrolysis that are currently being explored to accomplish this goal.

A fundamental prerequisite for improved pyrolysis yield and selectivity is clever chemical reaction engineering of the pyrolytic conversion, with the aim of ensuring optimal chemical pathways for biomass conversion. The present study is focused on fluidized bed fast pyrolysis, selected as a result of its versatility, robustness, and superior thermal performance over competing technologies as far as application to small-to-medium-scale decentralized plants for densification of raw biomass is addressed. Despite the inherent positive features of fluidized bed converters, particle heating and time−temperature history, biomass and volatile/gas residence times, gas and solid phase contacting, mixing, and flow pattern need to be carefully controlled to drive conversion along the prescribed chemical pathway.[16]

Mathematical modeling has been extensively used to support process and reactor development, and several modeling studies have addressed biomass pyrolysis in fluidized bed converters.[17−31] The course of primary biomass decomposition reactions and secondary homogeneous reactions of vapors have been largely unravelled by either compartmental models or computational fluid dynamics (CFD)-based approaches to elucidate the interactions between the complex multiphase dynamical patterns typical of fluidized beds and chemical reactions, represented through kinetic mechanisms and kinetics with variable degree of complexity. It is remarkable, however, that, when surveying the published literature on the subject, heterogeneous secondary reactions between volatile products of biomass decomposition and biomass char were most often overlooked in modeling fast pyrolysis of biomass as well as in the setup of process and reactor design guidelines. Kersten and co-workers[18,24] underlined that, especially at low temperatures, contact with char may overtake vapor residence time as the determinant for secondary cracking reactions of vapors generated by biomass decomposition. They recommended that char holdup in the pyrolyzer as well as the presence of entrained char in the hot parts of the reactor and the exhaust should be taken into account in reactor modeling and design. The lack of consideration of these aspects may affect the performance of the pyrolyzer as well as the reproducibility of results.

The topic of interaction of volatile matter from pyrolysis of solid fuels with the char residue has been frequently addressed in the literature. However, most contributions have been developed in the frame of tar reduction/control during biomass gasification, and quantitative knowledge concerning the volatile−char interaction at conditions relevant to fast pyrolysis is lacking. A seminal contribution has been given by Boroson et al.,[32] who were among the first to report extensive conversion of biomass (wood) pyrolysis vapors over fresh biomass char. They concluded that a fraction of biomass pyrolysis vapors is very reactive (even at very small contact times) in the presence of fresh biomass pyrolysis char at temperatures as low as 400 °C, yielding CO_2 and CO as products of char-induced tar conversion, with additional char (coke) as a highly probable product. The same fraction is fairly resistant to vapor-phase thermal cracking up to 600 °C. Lignin is indicated as a major but not the only source of this fraction.

Hoekstra et al.[33] have made a remarkable step forward along this direction by characterizing the effect of the vapor−char interaction at conditions relevant to fluidized bed pyrolysis of biomass. They found that char itself is not catalytically active inside the fluidized bed reactor, but the presence of minerals (Na/K), in either the biomass matrix or external (as salt or in char), does influence the fast pyrolysis process. They concluded that heterogeneous vapor-phase charring/polymerization reactions were more important than cracking reactions of vapors to gas in their experiments. They expressed the belief that "... a generic mathematical description of the pyrolysis reactions either leads to a dangerous oversimplification or to a model with far too many (unknown) fit parameters..." and that "... simple models based on measurable parameters supported by good understanding of the actual phenomena taking place (decomposition and vapor-phase reactions) allow for the most reliable prediction/extrapolation of the performance just outside the measured area for which the models were derived...".

Li et al.[34] provided additional evidence of the secondary heterogeneous interaction of primary products of lignin pyrolysis in a fluidized bed converter with sand replaced by lignin char as the bed material.

The bulk of studies on the volatile−char interactions confirm the influence of alkali and alkaline earth metals (AAEM) as effective catalysts of heterogeneous secondary reactions and highlight the difference between the newly formed "nascent" char and the *ex situ* fully stabilized char. Du et al.[35] report that the reactivity of the nascent char increased 2-fold in the presence of AAEM dispersed with the char matrix. Zhu et al.[36] report that secondary pyrolysis reactions resulted in the formation of low-molecular-weight derivatives, such as molecular acids, as a result of volatile−char interactions. The presence of potassium in the char also increased the rate of demethoxylation and demethylation of guaiacyl-containing structures, leading to the formation of phenols and the increased release of CH_4. Brown and co-workers[37−39] demonstrated the role of AAEM in catalyzing pyranose ring fragmentation in cellulose and hemicellulose that effectively hampered the production of sugars from biomass pyrolysis.

The catalytic nature of nascent chars for the pyrolysis heterogeneous secondary reaction is still poorly understood, although it is believed that it may play a major role in the reforming of volatiles to form condensable tars, along reaction pathways that involve oxygen-containing functional groups and the interaction between nascent char and the radicals generated during biomass pyrolysis.[40,41]

The recognition of the relevance of the heterogeneous vapor−char interaction to bio-oil production emphasizes the importance of proper control of char loading, establishing at steady state during operation of a fluidized bed biomass pyrolytic converter. Char holdup is regulated by the balance that occurs as fresh biomass is continuously fed, while some of the char is subject to entrainment and elutriation,[33,42] possibly enhanced by attrition.[16,43] Char carryover and elutriation may not be sufficient to prevent undesired char accumulation, and bed drain and *ex situ* regeneration, with removal of carbon-containing components, are most typically accomplished to control biomass and char inventories. Moreover, char residence time affects the "freshness" of nascent char and the availability of oxygen functionalities that may enhance the catalytic activity for low ash biomass feedstocks.[44] Plouffe et al.[39] recognized the relevance of char buildup in fluidized bed pyrolyzers to secondary conversion of pyrolysis vapors and

https://doi.org/10.1021/acs.energyfuels.2c01483
Energy Fuels 2022, 36, 9660−9671

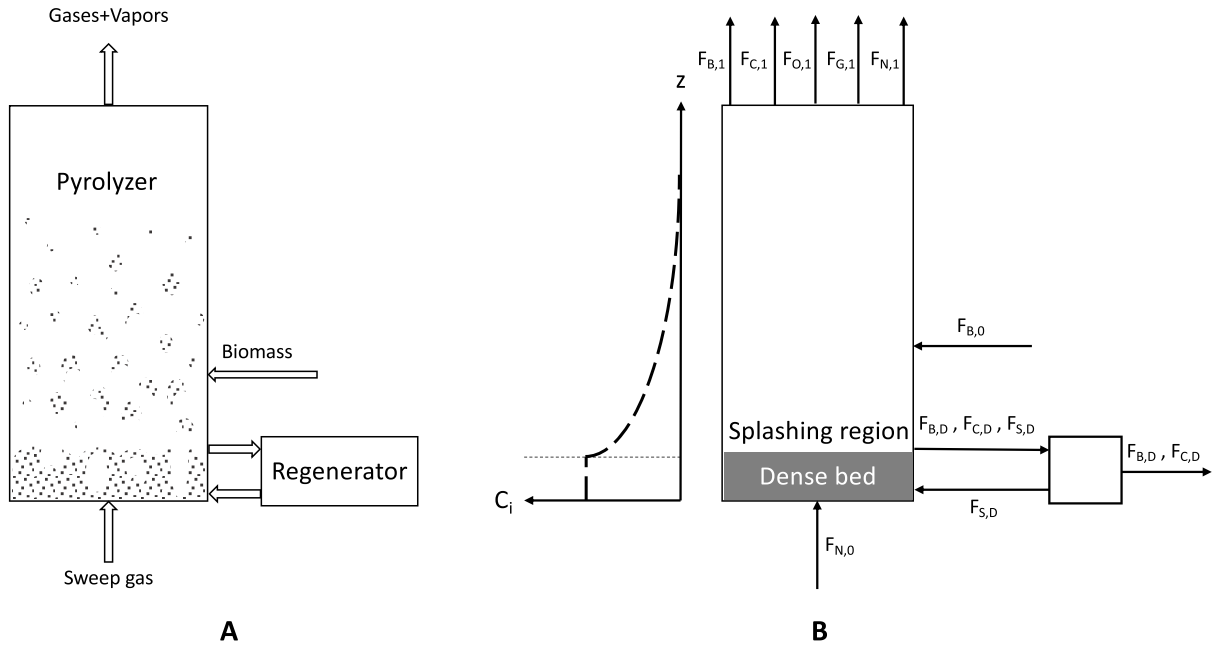

Figure 1. Fluidized bed pyrolytic converter.

analyzed the effect of overbed versus underbed biomass feeding on the bio-oil yield and speciation.

In the present study, a model-based assessment of the relevance of heterogeneous secondary reactions between pyrolysis vapors and biomass char is undertaken. To this end, a one-dimensional (1D) model based on a simplified, although comprehensive, representation of the key features of the fluidized bed pyrolytic converter has been developed, moving from preliminary results obtained with a simplified compartmental model.[45] The reactor design and operating conditions considered in the model have been selected to minimize the expected secondary interaction between primary products of biomass pyrolysis and the biochar. Accordingly, a shallow fluidized bed with overbed feeding of relatively fine biomass particles has been considered. The remarkable feature of the present mathematical model is careful consideration of processes that control the establishment of a steady char loading in the bed, namely, entrainment, elutriation, attrition, and bed drain/regeneration. Primary pyrolytic decomposition of biomass and secondary homogeneous reactions have been modeled using a semi-lumped reaction network, whose reliability has been widely recognized in the literature. Modeling the kinetics of the heterogeneous volatile−char secondary reaction step has been accomplished by borrowing a kinetic expression for the volatile−char interaction in the neighboring field of tar removal during fluidized bed gasification of biomass. Model results are helpful to shed light on the role of heterogeneous secondary reactions and the proper management of char loading during fluidized bed fast pyrolysis, providing useful criteria and guidelines for optimal design and operation of a fluidized bed pyrolytic converter.

2. MATHEMATICAL MODEL

2.1. Fluidized Bed Pyrolytic Converter. Figure 1A outlines the fluidized bed pyrolyzer assumed as a reference in the model setup. A shallow bubbling fluidized bed with overbed feeding of the biomass particles has been considered, with the goal of addressing conditions that hamper the secondary interaction of pyrolysis vapors with biochar. The reactor operates under steady-state conditions at atmospheric pressure. The temperature is uniform in the reactor, and thermal equilibrium among phases holds. The pyrolytic converter is modeled according to a 1D distributed parameter model (Figure 1B).

The small aspect ratio of the shallow dense bed and the excess of gas superficial velocity over incipient fluidization are responsible for a considerable fraction of bed solid holdup being located in the splashing region of the bed. The prevailing multiphase flow pattern is ejection/fall-back of bed particles promoted by bubbles and spouts bursting at the dense bed surface.[46−49] Accordingly, the gas phase is treated as a pseudo-homogeneous phase rather than a bubbly flow, and interphase mass transfer is ignored.

Bed hydrodynamics and solid holdup have been modeled by assuming that the bed solid inventory is split between a shallow dense bed and the splash zone (Figure 1). The axial concentration profile of the solid component i, where i = S (inert material), B (biomass), or C (char), has been expressed on the basis of experimental results and correlations developed at Chalmers University[50−52] as

$$C_i = \rho_{0i} e^{-a_i z} \quad i = \text{S, B, or C} \tag{1}$$

where the solid concentration decay coefficient a_i is given by

$$a_i = 4\frac{U_{t,i}}{U} \quad i = \text{S, B, or C} \tag{2}$$

Considering the combined effects of overbed particle feeding and biomass particle self-segregation during volatile release,[16,53,54] it is assumed that the biomass and char inventories in the dense bed are negligible. Accordingly, most of the biomass and char holdup are located in the splashing region, where, as a result of extensive particle entrainment and recirculation,[52,55] they can be considered well-stirred. The dense bed, if any, consists of the inert bed material, only. These assumptions are partly supported by results of Kohler et al.,[55,56] who report pronounced "stratification" and axial segregation of the lighter biomass and char particles in mixed beds of sand, biomass, and char, at least at the moderate gas superficial velocities that are usually established during fast pyrolysis in bubbling fluidized beds.

Within this general frame, a dense bed is formed provided that the inventory W_S of inert bed solids exceeds the maximum holdup of inert bed solids in the splash zone for the given gas superficial velocity.

$$W_S > \frac{S\rho_S(1-\varepsilon_{mf})}{a_S}[1 - e^{-a_S H}] \tag{3}$$

https://doi.org/10.1021/acs.energyfuels.2c01483
Energy Fuels 2022, 36, 9660−9671

In this case, the depth H_B of the dense bed is given by the condition

$$W_S = S\rho_S(1-\varepsilon_{mf})\left\{H_B + \frac{1}{a_S}[1-e^{-a_S(H-H_B)}]\right\} \quad (4)$$

If a dense bed is formed, the axial concentration profiles of the solid components along the bed are given by the following equations:

$$C_S(z) = \begin{cases} \rho_S(1-\varepsilon_{mf}) & H \le H_B \\ \rho_S(1-\varepsilon_{mf})e^{-a_S(z-H_B)} & H > H_B \end{cases} \quad (5)$$

$$C_i(z) = \begin{cases} 0 & H \le H_B \\ \rho_{0i}e^{-a_i(z-H_B)} & H > H_B \end{cases} \quad i = \text{B or C} \quad (6)$$

where ρ_{0i} is related to the inventory of the species i by the equation

$$W_i = \frac{S\rho_{0i}}{a_i}[1-e^{-a_i(H-H_B)}] \Rightarrow \rho_{0i} = \frac{W_i a_i}{S[1-e^{-a_i(H-H_B)}]} \quad i = \text{S, B, or C} \quad (7)$$

In the case that a dense bed is not formed, i.e., for $W_S \le \frac{S\rho_S(1-\varepsilon_{mf})}{a_S}[1-e^{-a_S H}]$, the axial concentration profiles of the solid components along the reactor are given by the equation

$$C_i(z) = \rho_{0i}e^{-a_i z} \quad i = \text{S, B, or C} \quad (8)$$

where ρ_{0i} is given by

$$W_i = \frac{S\rho_{0i}}{a_i}[1-e^{-a_i H}] \Rightarrow \rho_{0i} = \frac{W_i a_i}{S[1-e^{-a_i H}]} \quad i = \text{S, B, or C} \quad (9)$$

The profile of bed voidage along the reactor axis is given by

$$\varepsilon(z) = 1 - \sum_i \frac{C_i(z)}{\rho_i} \quad i = \text{S, B, or C} \quad (10)$$

where ρ_i is the particle density of the solid species i.

Computations have been performed by assuming a constant value of the total volume of solids V_{sol}, corresponding to a fixed value of the settled bed height H_{sb} that has been treated as an input parameter.

$$V_{sol} = \sum_i \frac{W_i}{\rho_i} = SH_{SB}(1-\varepsilon_{mf}) \quad i = \text{S, B, or C} \quad (11)$$

In this framework, all of the chemical reactions take place in the splash zone. The gas phase in the splash zone can be considered a pseudo-homogeneous medium. The gas flow pattern is modeled according to the axial dispersion model with variable mixture density and velocity, following the approach described by Douglas and Bischoff.[57] The axial dispersion coefficient is assumed constant and calculated considering the axially averaged value of the gas velocity.

Char accumulation in the bed is controlled by the continuous drain of bed solids, which is most conveniently accomplished at the surface of the bottom bed. Drained solids are eventually processed in a regenerator; hence, biomass-free bed material is recycled to the fluidized bed reactor. Biomass and char are removed from the inert bed material in the regenerator by either combustion or physical separation depending upon the intended further exploitation of the char.

2.2. Reaction Mechanisms and Kinetics: Biomass Decomposition and Homogeneous Secondary Reactions. A semi-lumped reaction scheme, similar to that suggested by Shafizadeh and Chin,[58] has been assumed in the model (Figure 2). The scheme considers the classical lumped species: gas (G), oil (O), and char (C), generated by primary pyrolysis of biomass (B). Secondary reactions 4 and 5 account for homogeneous cracking/rearrangement, condensation, and aromatization of oil to gas and/or char. Reaction 6 represents the lumped bundle of secondary heterogeneous reactions between vapors (O) and char.

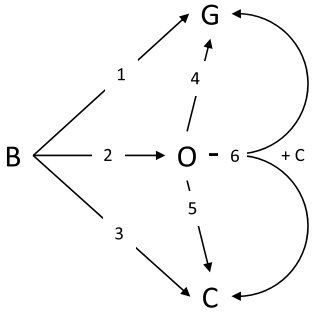

Figure 2. Semi-lumped reaction scheme.

Table 1 reports the kinetic parameters used in the model. The kinetics of primary reactions is modeled according to Di Blasi and Branca.[59] The kinetics of secondary homogeneous reactions 4 and 5 are modeled according to Liden et al.[60] and Di Blasi,[61] respectively.

Biomass particles are assumed to be small enough [Biot number (Bi) < 1] for the effect of particle shrinkage and intraparticle thermal non-uniformities to be negligible. Again, the choice of operating with small biomass particles, in the thermally thin regime, was dictated by the goal of addressing conditions that minimize secondary intraparticle interaction of pyrolysis vapors with nascent char. Accordingly, pyrolysis of biomass is described by the progressive conversion model: biomass particle size is constant, and its density decreases as a result of increasing porosity during the course of the reaction.[20] An independent preliminary assessment indicated that biomass conversion taking place during particle heating to the reference temperature of 500 °C at 1000 K s^{-1} is smaller than 5%. Accordingly, biomass conversion during particle heating was neglected in the computations.

2.3. Reaction Mechanisms and Kinetics: Heterogeneous Secondary Reactions. Steam gasification of char is negligible at the pyrolysis temperatures considered in the study. The bed material is inert and exerts no catalytic activity.

Despite the extensive evidence of the role of biochar and its constituents as catalysts/reagents in secondary reactions of pyrolysis vapors, there is a remarkable lack of quantitative information in the literature that may support modeling of the extraparticle vapor−char interaction. In the frame of the present study, information has been searched for in the neighboring areas of intraparticle vapor−char secondary reactions[62−64] and tar removal/decomposition by chars and carbons during biomass gasification.[32,65−70]

Analysis of correlations suggested for the intraparticle vapor−char interaction lead to values of $k_6 \approx 0.1-1$ m^3 kg^{-1} s^{-1} [62−64] at the temperature of 500 °C. Similar values are suggested by working out data obtained in mode 2 operation by Boroson et al.[32] (actually, even larger values would be estimated by data obtained in mode 4 operation).

Hosakai et al.[68] and Fuentes Cano et al.[70] provide quantitative correlations for the decomposition of biomass tars over charcoal, with a focus on aromatic compounds, in the frame of tar removal during biomass gasification. They clearly underline the sequential nature of tar abatement over charcoal: uptake and decomposition/coking of tar take place at first, followed by steam gasification of coke and char that reactivates charcoal reactivity. Extrapolation of Hosakai et al.[68] and Fuentes Cano et al.[70] data to 500 °C, the reference temperature assumed in the present study, suggests tar uptake rates consistent with $k_6 \approx 0.001$ m^3 kg^{-1} s^{-1} (benzene) to $k_6 \approx 0.01$ m^3 kg^{-1} s^{-1} (toluene and naphtalene). The same data indicate that steam gasification of the deposited and possibly coked tar does not take place to any significant extent at 500 °C.

No correlation is available in the literature for secondary reactions with biochar of non-aromatic biomass-derived tars. In particular, there is a remarkable lack of quantitative kinetic data and correlations for secondary heterogeneous reactions of heterocyclic compounds and sugars that largely contribute to the primary product of holocellulose

https://doi.org/10.1021/acs.energyfuels.2c01483
Energy Fuels 2022, 36, 9660−9671

Table 1. Kinetic Parameters

reaction	kinetics (kg m^{-3} s^{-1})	pre-exponential factor, $k_{0,i}$	activation energy, $E_{a,i}$ (kJ mol^{-1})	reference
$B \xrightarrow{1} \alpha_1 G$	$r_1 = k_1 C_B$	4.4×10^9 s^{-1}	153	59
$B \xrightarrow{2} \beta_2 O$	$r_2 = k_2 C_B$	1.1×10^{10} s^{-1}	148	59
$B \xrightarrow{3} \gamma_3 C$	$r_3 = k_3 C_B$	3.3×10^6 s^{-1}	112	59
$O \xrightarrow{4} \alpha_4 G$	$r_4 = k_4 \rho \omega_O$	4.3×10^6 s^{-1}	108	60
$O \xrightarrow{5} \gamma_5 C$	$r_5 = k_5 \rho \omega_O$	1×10^5 s^{-1}	108	61
$O \xrightarrow{6,+C} \alpha_6 G + \gamma_6 C$	$r_6 = k_6 C_C \rho \omega_O$	7.1 m^3 kg^{-1} s^{-1}	43	

pyrolysis. Sun et al.[41] indicate that aftertreatment of pyrolysis vapors in a charcoal bed at 500 °C yields comparable abatement of heterocyclic/alicyclic (furans and cyclopentenone) and aromatic (guaiacol and phenol) compounds, suggesting that charcoal is equally active toward a broad range of tars.

Altogether, with awareness of the broad uncertainties associated with kinetic modeling of heterogeneous reactions of different compounds with biochar and in light of the preliminary assessment character of the present studys, the rate of reaction 6 has been modeled using parameters reported in Table 1, obtained by working out Hosakai et al.[68] data for naphtalene deposition/coking on biochar. Stoichiometric coefficients were set at $\alpha_6 = 0.05$ and $\gamma_6 = 0.95$.

The above analysis raises the criticality of adequate characterization of mechanisms and rate of secondary reactions between pyrolysis vapors and biochar, with due consideration of the distinct classes of primary vapors at conditions relevant to biomass pyrolysis. This need will be further emphasized by analysis of the results of the present computations.

2.4. Material Balances. Material balance equations have been set on the four "active" components, namely, the raw biomass (B) and the pyrolysis products: char (C), oil (O), and gas (G). Material balances on the solid components (B and C) have been based on a well-stirred pattern hypothesis, consistent with the splash zone hydrodynamics outlined in section 2.1. An additional material balance has been set on the inert sweep gas (N).

material balance on biomass (B)

$$F_{B,0} - W_B(k_1 + k_2 + k_3) - F_{B,E} - F_{B,D} = 0 \tag{12}$$

$$F_{B,E} = F_{el,B} + F_{a,B} + F_{e,B} \tag{13}$$

material balance on char (C)

$$W_B \gamma_3 k_3 + R_{5,C} + R_{6,C} - F_{C,E} - F_{C,D} = 0 \tag{14}$$

where

$$F_{C,E} = F_{el,C} + F_{a,C} + F_{e,C} \tag{15}$$

and

$$R_{5,C} = \gamma_5 S \int_0^H k_5 \varepsilon \rho \omega_O \, dz \tag{16}$$

$$R_{6,C} = \gamma_6 S \int_0^H k_6 \rho \omega_O C_C \, dz \tag{17}$$

material balance on oil (O)

$$\frac{d(Q\rho\omega_O)}{dz} = S\bar{D}\frac{d}{dz}\left(\rho\frac{d\omega_O}{dz}\right) + S\beta_2 k_2 C_B - \varepsilon S k_4 \rho \omega_O - \varepsilon S k_5 \rho \omega_O - S k_6 \rho \omega_O C_C \tag{18}$$

material balance on gas (G)

$$\frac{d(Q\rho\omega_G)}{dz} = S\bar{D}\frac{d}{dz}\left(\rho\frac{d\omega_G}{dz}\right) + S\alpha_1 k_1 C_B + \varepsilon S\alpha_4 k_4 \rho \omega_O + S\alpha_6 k_6 \rho \omega_O C_C \tag{19}$$

material balance on sweep gas (N)

$$\frac{d}{dz}[Q\rho(1 - \omega_O - \omega_G)] = 0 \tag{20}$$

The boundary conditions associated with differential equations are

$$z = 0 \rightarrow Q = \frac{RT}{P}\frac{F_{N,0}}{PM_N}; \quad 0 = Q\rho\omega_O - S\bar{D}\rho\frac{d\omega_O}{dz}; \quad 0 = Q\rho\omega_G - S\bar{D}\rho\frac{d\omega_G}{dz}$$

$$z = H \rightarrow \frac{d\rho\omega_O}{dz} = \frac{d\rho\omega_G}{dz} = 0 \tag{21}$$

2.5. Constitutive Equations. All compounds in the gas phase behave as ideal gases, and the density of the mixture is calculated accordingly.

$$\rho = \frac{P}{RT}\frac{1}{\sum_i \frac{\omega_i}{M_i}} \quad i = O, G, \text{ or } N \tag{22}$$

It is assumed that the particle leaving the reactor in the effluent gas is derived from three contributions: elutriated particles, i.e., particles that are carried over in the gaseous stream even beyond the transport disengagement height (TDH); attrited fines, i.e., particles generated by attrition by abrasion, fine enough to be immediately carried over to the reactor exhaust; and entrained particles, i.e., particles reaching the reactor exhaust as a result of the splashing mechanism. Expressions for these three contributions are hereby given.

Elutriation of biomass and char particles is evaluated by the following equation:

$$F_{el,i} = k_{el,i} W_i \quad i = B \text{ or } C \tag{23}$$

where

$$k_{el,i} = K^*_{i,\infty}\frac{S}{\sum_j W_j} \quad i = B \text{ or } C; \quad j = S, B, \text{ or } C \tag{24}$$

The expression of the elutriation flux constant $K^*_{i,\infty}$ proposed by Geldart et al.[71,72] is assumed.

$$\frac{K^*_{i,\infty}}{\rho_g U} = 23.7 \exp\left(-5.4\frac{U_{t,i}}{U}\right) \quad i = B \text{ or } C \tag{25}$$

Attrition by abrasion of biomass particles is neglected ($F_{a,B} = 0$). Attrition of char particles is modeled assuming the constitutive equation and the attrition constant $k_{a,C}$ proposed by Scala et al.[43]

https://doi.org/10.1021/acs.energyfuels.2c01483
Energy Fuels 2022, 36, 9660−9671

$$F_{a,C} = k_{a,C}\frac{U - U_{mf}}{d_{p,C}}W_C \quad (26)$$

Accordingly, the attrition rate is directly proportional to char inventory and the excess gas superficial velocity with respect to the incipient fluidization velocity and is inversely proportional to char particle size.

Entrainment of particles at the reactor exhaust has been calculated as the product of the concentration of solid species and the volumetric flow rate at $z = H$.

$$F_{e,i} = (QC_i)|_H \quad i = \text{S, B, or C} \quad (27)$$

Control of biomass and char inventory may require bed drain and regeneration in the external regeneration unit (Figure 1). On the basis of the assumption that solids are well-stirred, the concentration of each solid component in the bed is considered equal to that in the drainage. Hence, the space time τ_D, the ratio of the solid inventory and the solid drain rate, is the same for all solid components.

$$\tau_D = \frac{W_i}{F_{i,D}} = \frac{\sum_i W_i}{\sum_i F_{i,D}} \quad i = \text{S, B, or C} \quad (28)$$

Constitutive equations are complemented by correlations for the minimum fluidization velocity U_{mf} of the bed material and the terminal velocity $U_{t,i}$ of each solid component taken from Wen and Yu[73] and Haider and Levenspiel,[74] respectively.

2.6. Solution Procedure. The model equations consist of an algebraic−differential system of equations coupled with each other. Differential equations were solved using a numerical procedure based on a four-stage orthogonal collocation method. The computational procedure requires trial-and-error iterations for biomass and char inventories, whose convergence turned out to be straightforward. The computational code was implemented in the MATLAB environment.

3. RESULTS AND DISCUSSION

3.1. Selection of Input Parameters for Base Case Computations. Values of the attrition constant, properties of the fluid and solid components, and other input parameters for the base case model computations are reported in Table 2. Model computations have been based on the assumption that the sweep gas consists of technical-grade nitrogen. Stoichiometric coefficients in Table 1 were all set equal to 1, with the exception of α_6 and γ_6.

The axial dispersion coefficient has been estimated on the basis of published data regarding hydrodynamics and mixing patterns in the splash regions of bubbling fluidized beds.[75−78] In particular, following Solimene et al.,[77,78] a value of $D = 1 \times 10^{-3}$ m^2 s^{-1} has been assumed.

The biomass-to-sweep gas feed rate of the pyrolyzer was set at values typical of the operating conditions of bubbling fluidized bed pyrolyzers reported from the literature.[33,39]

The selection of the total height H of the converter and the operating gas superficial velocity U has been made on the basis of preliminary results of model computations. Results of oil and gas yields are reported in Figure 3 as a function of the gas superficial velocity U for different values of the gas space time τ_g, defined as $(H-H_{SB})/U$.

Table 2. Model Input Parameters for Base Case Computations

parameter	value
P (atm)	1
T (K)	773
$\bar{D}$ (m^2 s^{-1})	0.001
H (m)	0.5
H_{sb} (m)	0.2
S (m^2)[a]	0.04
U (m s^{-1})	0.3
d_p (μm)	500
d_S (μm)	500
$U_{mf,S}$ (m s^{-1})	0.12
$U_{t,B}$ (m s^{-1})	2.2
$U_{t,C}$ (m s^{-1})	0.81
$k_{a,C}$	3×10^{-7}
$F_{B,0}$ (kg s^{-1})	0.0042
$F_{N,0}$ (kg s^{-1})	0.027
Q (Nm^3 s^{-1})	0.0042
ρ_B (kg m^{-3})	1000
ρ_C (kg m^{-3})	300
ρ_S (kg m^{-3})	2600

[a]A 0.2 × 0.2 m^2 cross section.

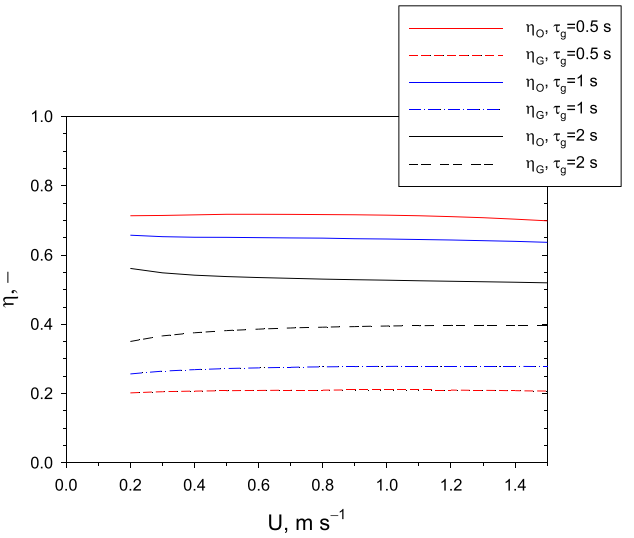

Figure 3. Oil and gas yields as a function of the gas superficial velocity for fixed values of the gas space time in the pyrolyzer.

Computations have been performed for a fixed value of drainage space time, $\tau_D = 100$ s, far exceeding typical reaction time scales of fast pyrolysis reactions (≈1 s). The gas and oil yields are fairly costant with increasing gas superficial velocity for all of the values of τ_g investigated. Small departures from the constant trend are due to small changes in the effective gas residence time as bed solid loading profiles along the reactor change, affecting the extent of homogeneous secondary gas-phase reactions.

To maximize η_O while keeping a reasonable excess of gas velocity with respect to the incipient fluidization velocity of the inert bed material, the gas superficial velocity was set at $U = 0.3$ m/s in the reference base case computations. In Figure 3, it is noteworthy that the highest values of η_O are obtained for $\tau_g = 0.5$ s, consistent with an overall height of the pyrolyzer of $H = 0.35$ m. However, for this value of H, it is found that nearly 5% of the raw biomass feeding is entrained from the bed, with penalties in terms of the loss of fuel and additional charge to the solid separation units. On the other hand, for $\tau_g = 1$ s, the oil yield is only marginally lower and no biomass is entrained from the converter. For this reason, a reference value of $\tau_g = 1$ s has been considered for the model computations, and the pyrolyzer height has been correspondingly set at $H = 0.5$ m.

https://doi.org/10.1021/acs.energyfuels.2c01483
Energy Fuels 2022, 36, 9660−9671

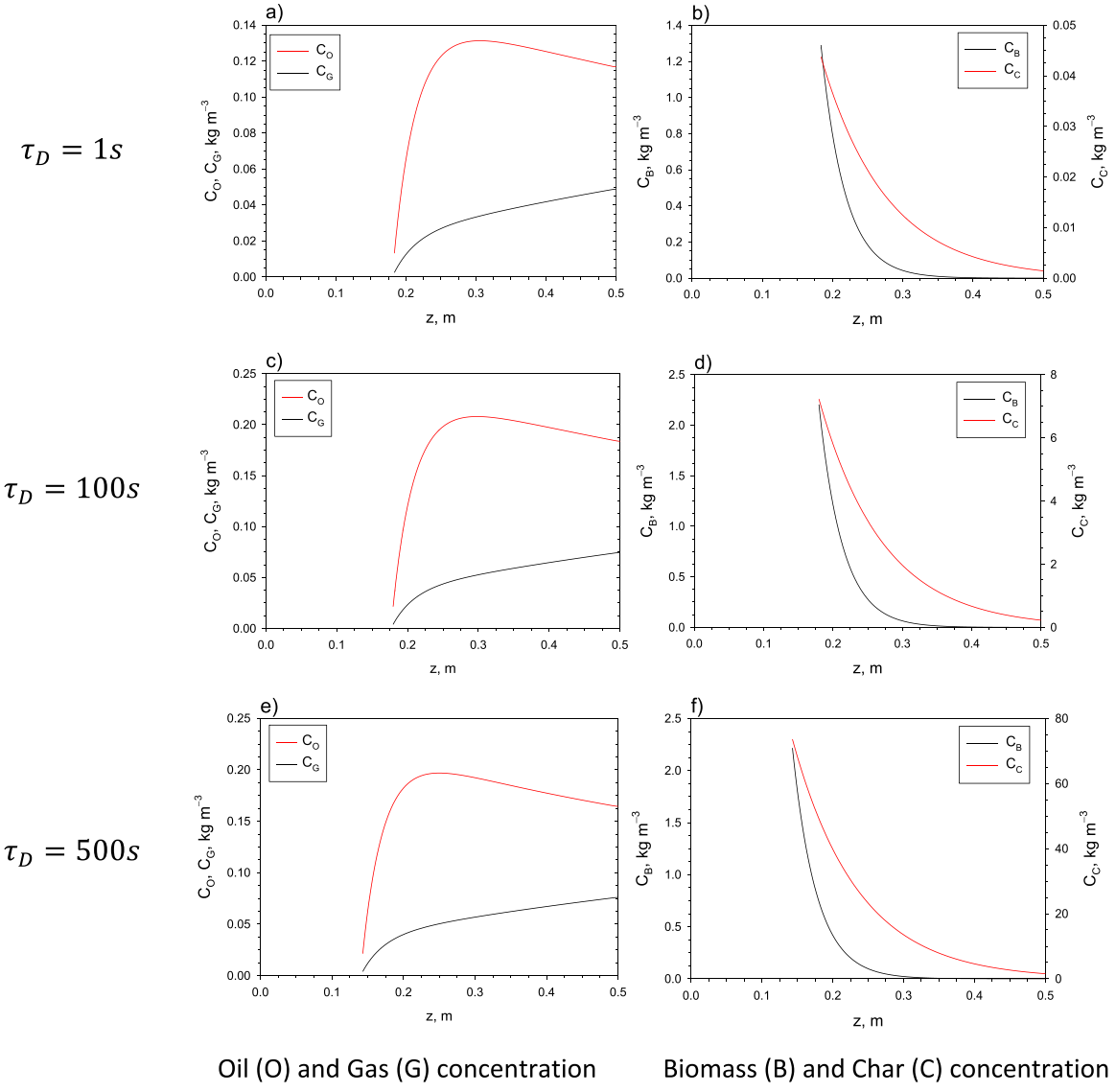

Figure 4. Axial concentration profiles of oil and gas for (a) τ_D = 1 s, (c) τ_D = 100 s, and (e) τ_D = 500 s. Axial concentration profiles of biomass and char for (b) τ_D = 1 s, (d) τ_D = 100 s, and (f) τ_D = 500 s.

3.2. Results for Base Case Computations. Selected axial concentration profiles of oil, gas, biomass, and char are reported in Figure 4. Data are referred to the base case operating conditions, considering drainage space times ranging between τ_D = 1 and 500 s. Detailed inspection of profiles indicates that the concentrations of all of the species are equal to zero up to an axial coordinate $z \cong 0.15-0.18$ m, corresponding to the dense bed height H_B that is established for the given gas superficial velocity and overall bed inventory. The oil concentration reaches a maximum value for $z \cong 0.3$ m for τ_D = 1 s, to decrease thereafter along the axial coordinate of the converter as a consequence of secondary reactions. The peak values of C_O are 0.13 kg m^{-3} for τ_D = 1 s, 0.21 kg m^{-3} for τ_D = 100 s, and 0.2 kg m^{-3} for τ_D = 500 s and are attained at the levels where the biomass concentration vanishes (see panels b, d, and f of Figure 4). On the other hand, the gas concentration C_G increases monotonically along the reactor length for all of the drainage space times considered.

With regard to the solid concentration profiles, both biomass and char concentrations decrease along the axial coordinate of the converter starting from the height H_B. It is noteworthy that, for τ_D = 1 s, char inventory in the bed is fairly small, with a char loading per unit cross-sectional area of 0.004 kg m^{-2}, consistent with the vanishingly small char concentration profile in Figure 4b. The char loading per unit bed cross section increases to 0.76 kg m^{-2} for τ_D = 100 s (Figure 4d) and 6.85 kg m^{-2} for τ_D = 500 s (Figure 4f). A similar trend is observed for the biomass B component, with maximum concentrations of 1.3, 2.2, and 2.22 kg m^{-2} for τ_D = 1, 100, and 500 s, respectively.

As far as the relationship between η_O and τ_D is concerned, the phenomenology closely reflects the competing effects of oil production by biomass decomposition (reaction 2 in Figure 2) and secondary conversion of oil as a result of homogeneous (reactions 4 and 5) and heterogeneous (reaction 6) secondary reactions. At very small values of τ_D, i.e., for large values of the bed drain rate, biomass conversion to oil along reaction path 2

https://doi.org/10.1021/acs.energyfuels.2c01483
Energy Fuels 2022, 36, 9660−9671

is incomplete. For large values of τ_D, the heterogeneous vapor−biochar reaction overtakes oil generation. An optimal value of τ_D, $\tau_D \approx 100$ s in the base case computations, corresponds to the maximum bio-oil yield η_O.

3.3. Effect of the Biomass Particle Diameter. The effect of biomass and the closely related char particle size on oil and gas yields is reported in Figure 5 as a function of τ_D. For d_p =

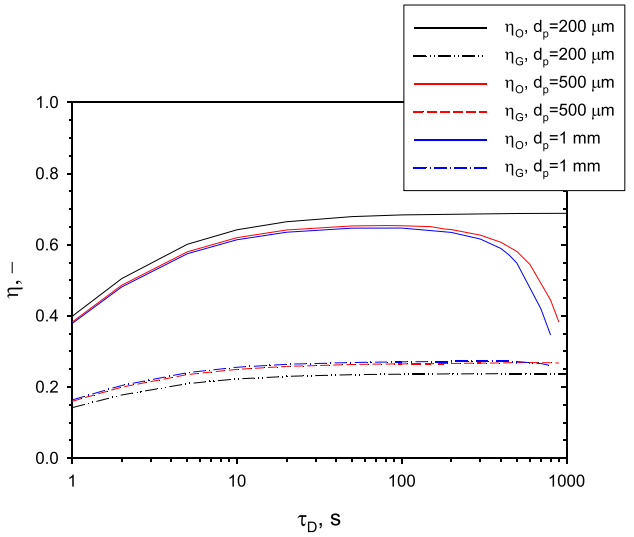

Figure 5. Oil and gas yields as a function of the drainage space time for different values of the biomass particle size.

200 μm, η_O and η_G increase with τ_D to reach a constant value of about 0.69 and 0.24, respectively. For d_p = 500 μm and 1 mm, η_O first increases to a maximum value and then, for τ_D larger than about 100 s, decreases. These trends can be explained if the concurrent paths responsible for char leaving the bed are taken into account. In fact, attrition by abrasion dominates over elutriation and is the dominant process balancing char accumulation for large drainage space times, such as larger than 500 s.

For small values of τ_D, char drainage overtakes abrasion as the process controlling char accumulation and holdup. The small value of char loading in the bed established under these conditions is consistent with a limited effect of heterogeneous secondary reactions. As a matter of fact, η_O^{max} assumes nearly the same value for all of the particle sizes investigated. Instead, for large values of τ_D, the oil yield decreases with an increasing particle size. This is due to a smaller abrasion rate as the particle size is increased, resulting in a larger char inventory in the bed. In fact, for τ_D = 10 s, the char loading is 0.01, 0.07, and 0.07 kg m^{-2} for d_p = 200 μm, 500 μm, and 1 mm, respectively, while for τ_D = 500 s, it is 0.02, 6.85, and 9.17 kg m^{-2} for d_p = 200 μm, 500 μm, and 1 mm, respectively.

Secondary heterogeneous reactions are emphasized, and the oil yield decreases for large values of τ_D. The gas yield is only moderately affected by the particle size at large drainage space times. This is most likely the consequence of the stoichiometry (α_6 = 0.05 and γ_6 = 0.95) assumed in the computations, which is consistent with a predominant yield to C rather than G as oil undergoes heterogeneous secondary conversion along the reaction path 6.

3.4. Effect of the Attrition Rate. The sensitivity of oil and gas yields on the value of the char attrition constant is reported in Figure 6 as a function of τ_D. Computations have been

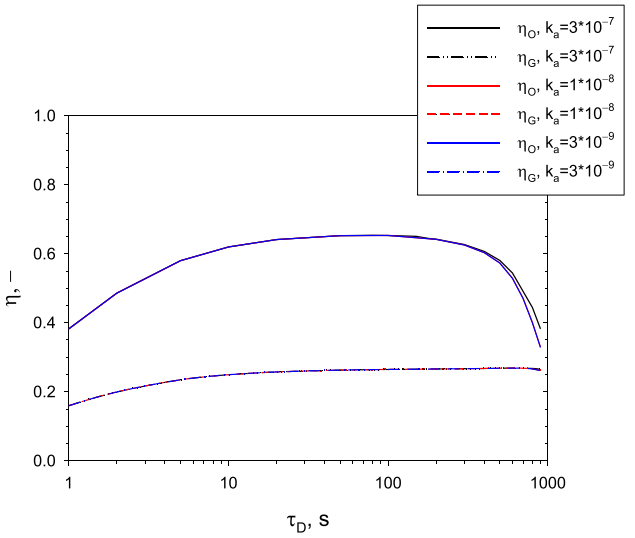

Figure 6. Oil and gas yields as a function of the drainage space time for different values of the char abrasion constant.

carried out assuming typical values of $k_{a,C}$ reported in the literature for three kinds of biomass: wood chips ($k_{a,C} = 3 \times 10^{-7}$), pine seed shells ($k_{a,C} = 1 \times 10^{-8}$), and olive husks ($k_{a,C} = 3 \times 10^{-9}$).[43] Oil yields reach the maximum value for τ_D at around 80 s for all of the values of $k_{a,C}$ considered. Thereby, η_O reaches a plateau and slightly decreases thereafter for large values of the drainage space time. In fact, the effect of the abrasion constant on the oil yield starts to be evident for τ_D larger than 500 s, with η_O decreasing for smaller values of the abrasion constant. This result highlights the role of attrition by abrasion on char loading in the bed and, accordingly, the effect of secondary heterogeneous reactions on product yields. For τ_D smaller than about 500 s, attrition by abrasion does not influence yields to a significant extent, because, for the selected values of $k_{a,C}$, the change in char loading as a result of abrasion is largely overcome by bed drain. On the other hand, the gas yield increases with τ_D to remain nearly constant. Henceforth, for τ_D larger than 500 s, the gas yield is nearly independent from the value of $k_{a,C}$, because, for very high τ_D, secondary reactions have a limited impact on the gas yield.

3.5. Effect of the Biomass-to-Sweep Gas Feed Ratio. The effect of the biomass-to-sweep gas feed ratio (B/SG) on oil and gas yields is reported in Figure 7 as a function of τ_D. B/SG has been varied by changing the biomass feed rate while keeping the sweep gas superficial velocity and the other operating conditions unchanged.

A non-monotonic trend of η_O is again observed as a function of τ_D. Maxima of η_O increase moderately with increasing B/SG and are located at values of τ_D that decrease as B/SG increases. In fact, the maximum values of η_O are obtained for τ_D = 20, 80, and 200 s for biomass-to-sweep gas feed ratios equal to 10, 1, and 0.1 kg Nm^{-3}, respectively.

Gas yields increase with the drainage space time and for decreasing values of B/SG.

The most remarkable feature of plots in Figure 7 is the variable range of τ_D, within which steady operation of the pyrolyzer may be established. For the largest value of B/SG investigated (=10 kg Nm^{-3}), stable operation can be achieved only for values of τ_D smaller than 100 s: when τ_D is set at values longer than 100 s, char inventory surges, making steady operation unsustainable. The range of steady operation

https://doi.org/10.1021/acs.energyfuels.2c01483
Energy Fuels 2022, 36, 9660−9671

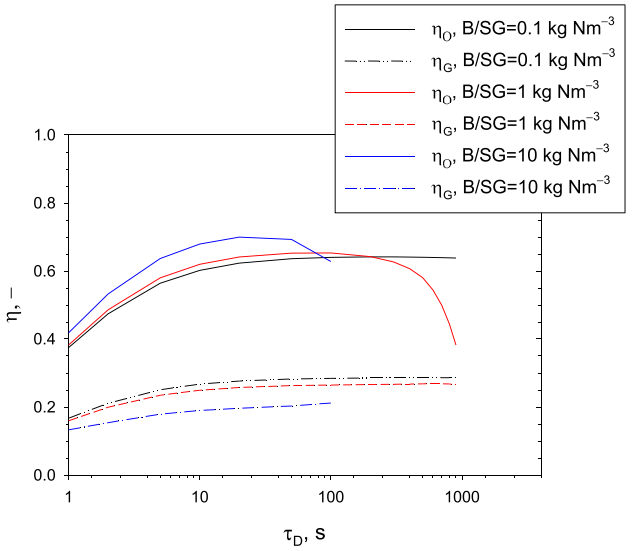

Figure 7. Oil and gas yields as a function of the drainage space time for different values of the biomass-to sweep gas feed ratio (B/SG).

expands to τ_D smaller than 500 s when B/SG is set at 1 kg Nm^{-3}.

3.6. Effect of the Temperature. Analysis of the effect of the temperature on oil and gas yields is reported in Figure 8 as

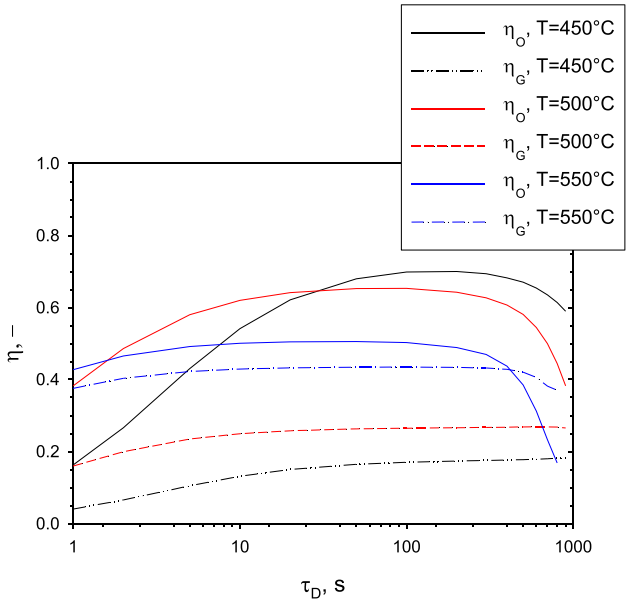

Figure 8. Oil and gas yields as a function of the drainage space time for different values of the operating temperature.

a function of τ_D. Oil yields display the typical non-monotonic trend as a function of τ_D, which, however, is much more pronounced at the lowest temperature of 450 °C than at the larger temperatures of 500 and 550 °C. Figure 8 indicates that η_O(450 °C) < η_O(500 °C) < η_O(550 °C) at very small values of τ_D, whereas the order is reversed η_O(550 °C) < η_O(500 °C) < η_O(450 °C) for large values of τ_D.

The observed trends of η_O may be interpreted in light of the competing effects of biomass decomposition to oil (reaction 2, characterized by the largest activation energy, ≅150 kJ mol^{-1}) and the parallel course of secondary reactions of oil to char and gas (homogeneous reactions 4 and to a lesser extent 5, characterized by activation energies of ≅110 kJ mol^{-1}, and heterogeneous reaction 6, with activation energy ≅43 kJ mol^{-1}).

For small values of τ_D, hence, a short biomass residence time in the converter, the oil yield is determined by the rate of biomass decomposition to oil (reaction 2), increasing with an increasing temperature.

For large values of τ_D, corresponding to long residence times of biomass particles in the pyrolyzer, biomass decomposition may be considered complete and the oil yield is controlled by the rate of secondary oil conversion to gas and char, whose extent increases with the operation temperature, resulting in η_O decreasing with an increasing temperature. The relative importance of homogeneous versus heterogeneous pathways to bio-oil degradation depends upon the temperature, with the homogeneous path being comparatively favored at a higher temperature and char holdup increasing with τ_D and enhancing the heterogeneous path.

Interpretation of the computed trends of gas yields η_G is more straightforward: gas is an end product of the complex network of series–parallel primary and secondary reactions. Hence, η_G increases steadily with the drainage space time τ_D and increases with the temperature as well, being η_G(450 °C) < η_G(500 °C) < η_G(550 °C) at any value of τ_D.

4. CONCLUSION

The mathematical model developed in the present study aimed at contributing, at least partly, to fill an apparent gap in the current understanding and predictive ability of fluidized bed pyrolysis of biomass: the relevance of *in situ* heterogeneous chemical reactions between pyrolysis vapors and biochar. Closely related with this issue is the assessment of the char loading that is established in the bed under the combined effects of char entrainment and elutriation, possibly enhanced by attrition, and bed material drain and regeneration. These processes have been modeled using constitutive equations selected from the literature. Solid entrainment, recirculation and holdup, and gas mixing were modeled considering hydrodynamical patterns typical of the splash region of shallow fluidized beds. A well-established semi-lumped kinetic mechanism has been used to model biomass decomposition and homogeneous secondary reactions of pyrolysis vapors.

The kinetics of heterogeneous vapor–char reactions represents an area of considerable uncertainty and a lack of available information. Preliminary assessment of the effect of secondary vapor–biochar reactions has been accomplished in the present study by analyzing the literature pertinent to the neighboring field of tar removal over biochar during biomass gasification.

Results of model computations pinpoint the relevance of char–vapor secondary reactions and the magnitude of bed char inventory to bio-oil and gas yields. The model provides a simple tool to optimize management of char loading through bed drain/regeneration toward a maximum bio-oil yield. A sensitivity analysis with respect to gas superficial velocity, gas residence time, biomass particle size, biomass-to-sweep gas feed ratio, and operating temperature is helpful to develop criteria and guidelines for optimal design and selection of operating conditions of fluidized bed pyrolytic converters.

Altogether, results of the present study confirm that improved knowledge of the mechanisms and kinetics of heterogeneous vapor–char reactions, and the development of a

https://doi.org/10.1021/acs.energyfuels.2c01483
Energy Fuels 2022, 36, 9660–9671

better predictive ability of char loading under conditions relevant to fluidized bed pyrolysis should be prioritized.

AUTHOR INFORMATION

Corresponding Author

Piero Salatino − *Dipartimento di Ingegneria Chimica, dei Materiali e della Produzione Industriale, Università degli Studi di Napoli Federico II, 80125 Napoli, Italy; Istituto di Scienze e Tecnologie per l'Energia e la Mobilità Sostenibili (STEMS), Consiglio Nazionale delle Ricerche, 80125 Napoli, Italy;* orcid.org/0000-0002-0002-1691; Email: piero.salatino@unina.it

Authors

Maurizio Troiano − *Dipartimento di Ingegneria Chimica, dei Materiali e della Produzione Industriale, Università degli Studi di Napoli Federico II, 80125 Napoli, Italy; Istituto di Scienze e Tecnologie per l'Energia e la Mobilità Sostenibili (STEMS), Consiglio Nazionale delle Ricerche, 80125 Napoli, Italy*

Valeria Ianzito − *Dipartimento di Ingegneria Chimica, dei Materiali e della Produzione Industriale, Università degli Studi di Napoli Federico II, 80125 Napoli, Italy*

Roberto Solimene − *Istituto di Scienze e Tecnologie per l'Energia e la Mobilità Sostenibili (STEMS), Consiglio Nazionale delle Ricerche, 80125 Napoli, Italy*

Elvis Tinashe Ganda − *Dipartimento di Ingegneria Chimica, dei Materiali e della Produzione Industriale, Università degli Studi di Napoli Federico II, 80125 Napoli, Italy;* orcid.org/0000-0003-1761-1329

Complete contact information is available at: https://pubs.acs.org/10.1021/acs.energyfuels.2c01483

Notes

The authors declare no competing financial interest.

ACKNOWLEDGMENTS

This study has been carried out in the frame of the Project PON ARS01_00985: Biofeedstock: Development of Integrated Technological Platforms for Residual Biomass Exploitation, funded by the Italian Ministry for University and Research. Elvis Tinashe Ganda acknowledges a grant from ENI for a Ph.D. position at Università degli Studi di Napoli Federico II as a recipient of the ENI Award Young Talents from Africa 2018. The authors acknowledge useful discussions with Paola Brachi, Riccardo Chirone, Roberto Chirone, Antonio Coppola, Renata Migliaccio, Giovanna Ruoppolo, Fabrizio Scala, Osvalda Senneca, and Massimo Urciuolo.

NOMENCLATURE

Symbols

a = concentration decay coefficient (m^{-1})
B/SG = biomass-to-sweep gas feed ratio (kg Nm^{-3})
C = mass concentration (kg m^{-3})
D = axial dispersion coefficient (m^2 s^{-1})
d_p = biomass and char particle diameter (m)
d_S = bed inert particle diameter (m)
E_a = activation energy (kJ mol^{-1})
F = mass flow rate (kg s^{-1})
H = height of the converter (m)
H_B = dense bed height (m)
H_{sb} = settled bed height (m)
k = kinetic rate constant
$k_{0,j}$ = pre-exponential factor of the jth reaction (s^{-1})
k_{el} = elutriation rate constant (s^{-1})
$K^*_{i,\infty}$ = elutriation flux constant for the ith species (kg m^{-2} s^{-1})
M = molecular weight (kg $kmol^{-1}$)
P = pressure (atm)
Q = volumetric gas flow rate (m^3 s^{-1})
r = reaction rate (kg m^{-3} s^{-1})
R = universal ideal gas constant (J mol^{-1} K^{-1})
$R_{j,i}$ = axially averaged reaction rate (kg s^{-1})
S = bed cross-sectional area (m^2)
T = temperature (K)
U = inlet gas superficial velocity (m s^{-1})
V = volume (m^3)
V_{sol} = total volume of solids (m^3)
W = mass (kg)
z = axial coordinate (m)

Greek Letters

α = stoichiometric coefficient of the gas phase
β = stoichiometric coefficient of the biomass phase
γ = stoichiometric coefficient of the char phase
ε = voidage
η = yield
ρ = density (kg m^{-3})
τ = space time (s)
ω = mass fraction

Subscripts

0 = relative to the inlet
a = relative to attrition by abrasion
B = biomass
C = char
D = drainage
e = entrainment
E = exit
g = gas phase
G = pyrolysis gas
i = species number
j = reaction number
mf = minimum fluidization
N = sweep gas
O = oil
S = inert bed material, solids
t = terminal

REFERENCES

(1) Hassan, S. S.; Williams, G. A.; Jaiswal, A. K. Lignocellulosic Biorefineries in Europe: Current State and Prospects. *Trends Biotechnol.* **2019**, *37* (3), 231−234.

(2) Bridgwater, A. V. Pyrolysis of Solid Biomass: Basics, Processes, and Products. In *Encyclopedia of Sustainability Science and Technology*; Meyers, R. A., Ed.; Springer: New York, 2017; pp 1−30, DOI: 10.1007/978-1-4939-2493-6_984-1.

(3) Kang, K.; Klinghoffer, N. B.; ElGhamrawy, I.; Berruti, F. Thermochemical Conversion of Agroforestry Biomass and Solid Waste Using Decentralized and Mobile Systems for Renewable Energy and Products. *Renewable Sustainable Energy Rev.* **2021**, *149*, 111372.

(4) Huber, G. W.; Iborra, S.; Corma, A. Synthesis of Transportation Fuels from Biomass: Chemistry, Catalysts, and Engineering. *Chem. Rev.* **2006**, *106* (9), 4044−4098.

(5) Anca-Couce, A. Reaction Mechanisms and Multi-Scale Modelling of Lignocellulosic Biomass Pyrolysis. *Prog. Energy Combust. Sci.* **2016**, *53*, 41−79.

(6) Wang, S.; Dai, G.; Yang, H.; Luo, Z. Lignocellulosic Biomass Pyrolysis Mechanism: A State-of-the-Art Review. *Prog. Energy Combust. Sci.* **2017**, *62*, 33−86.
(7) Yogalakshmi, K. N.; Poornima Devi, T.; Sivashanmugam, P.; Kavitha, S.; Yukesh Kannah, R.; Varjani, S.; AdishKumar, S.; Kumar, G.; Rajesh Banu, J. Lignocellulosic Biomass-Based Pyrolysis: A Comprehensive Review. *Chemosphere* **2022**, *286* (P2), 131824.
(8) Czernik, S.; Bridgwater, A. V. Overview of Applications of Biomass Fast Pyrolysis Oil. *Energy Fuels* **2004**, *18* (2), 590−598.
(9) Olazar, M.; Aguado, R.; Bilbao, J.; Barona, A. Pyrolysis of Sawdust in a Conical Spouted-Bed Reactor with a HZSM-5 Catalyst. *AIChE J.* **2000**, *46* (5), 1025−1033.
(10) Carlson, T. R.; Cheng, Y.-T.; Jae, J.; Huber, G. W. Production of Green Aromatics and Olefins by Catalytic Fast Pyrolysis of Wood Sawdust. *Energy Environ. Sci.* **2011**, *4* (1), 145−161.
(11) Paasikallio, V.; Agblevor, F.; Oasmaa, A.; Lehto, J.; Lehtonen, J. Catalytic Pyrolysis of Forest Thinnings with ZSM-5 Catalysts: Effect of Reaction Temperature on Bio-Oil Physical Properties and Chemical Composition. *Energy Fuels* **2013**, *27* (12), 7587−7601.
(12) Yildiz, G.; Ronsse, F.; van Duren, R.; Prins, W. Challenges in the Design and Operation of Processes for Catalytic Fast Pyrolysis of Woody Biomass. *Renewable Sustainable Energy Rev.* **2016**, *57*, 1596−1610.
(13) Hernando, H.; Gómez-Pozuelo, G.; Botas, J. A.; Serrano, D. P. Evaluating Fractional Pyrolysis for Bio-Oil Speciation into Holocellulose and Lignin Derived Compounds. *J. Anal. Appl. Pyrolysis* **2021**, *154*, 105019.
(14) Luque, L.; Westerhof, R.; Van Rossum, G.; Oudenhoven, S.; Kersten, S.; Berruti, F.; Rehmann, L. Pyrolysis Based Bio-Refinery for the Production of Bioethanol from Demineralized Ligno-Cellulosic Biomass. *Bioresour. Technol.* **2014**, *161*, 20−28.
(15) Wang, Z.; Burra, K. G.; Lei, T.; Gupta, A. K. Co-Pyrolysis of Waste Plastic and Solid Biomass for Synergistic Production of Biofuels and Chemicals-A Review. *Prog. Energy Combust. Sci.* **2021**, *84*, 100899.
(16) Salatino, P.; Solimene, R. Mixing and Segregation in Fluidized Bed Thermochemical Conversion of Biomass. *Powder Technol.* **2017**, *316*, 29−40.
(17) Lathouwers, D.; Bellan, J. Yield Optimization and Scaling of Fluidized Beds for Tar Production from Biomass. *Energy Fuels* **2001**, *15* (5), 1247−1262.
(18) Kersten, S. R. A.; Wang, X.; Prins, W.; van Swaaij, W. P. M. Biomass Pyrolysis in a Fluidized Bed Reactor. Part 1: Literature Review and Model Simulations. *Ind. Eng. Chem. Res.* **2005**, *44* (23), 8773−8785.
(19) Blanco, A.; Chejne, F. Modeling and Simulation of Biomass Fast Pyrolysis in a Fluidized Bed Reactor. *J. Anal. Appl. Pyrolysis* **2016**, *118*, 105−114.
(20) Hejazi, B.; Grace, J. R.; Bi, X.; Mahecha-Botero, A. Coupled Reactor and Particle Model of Biomass Drying and Pyrolysis in a Bubbling Fluidized Bed Reactor. *J. Anal. Appl. Pyrolysis* **2016**, *121*, 213−229.
(21) Peters, J. F.; Banks, S. W.; Bridgwater, A. V.; Dufour, J. A Kinetic Reaction Model for Biomass Pyrolysis Processes in Aspen Plus. *Appl. Energy* **2017**, *188*, 595−603.
(22) Lopez, G.; Alvarez, J.; Amutio, M.; Hooshdaran, B.; Cortazar, M.; Haghshenasfard, M.; Hosseini, S. H.; Olazar, M. Kinetic Modeling and Experimental Validation of Biomass Fast Pyrolysis in a Conical Spouted Bed Reactor. *Chem. Eng. J.* **2019**, *373*, 677−686.
(23) Chen, T.; Ku, X.; Lin, J.; Ström, H. CFD-DEM Simulation of Biomass Pyrolysis in Fluidized-Bed Reactor with a Multistep Kinetic Scheme. *Energies* **2020**, *13* (20), 5358.
(24) Wang, X.; Kersten, S. R. A.; Prins, W.; van Swaaij, W. P. M. Biomass Pyrolysis in a Fluidized Bed Reactor. Part 2: Experimental Validation of Model Results. *Ind. Eng. Chem. Res.* **2005**, *44* (23), 8786−8795.
(25) Luo, Z.; Wang, S.; Cen, K. A Model of Wood Flash Pyrolysis in Fluidized Bed Reactor. *Renewable Energy* **2005**, *30* (3), 377−392.
(26) Papadikis, K.; Gu, S.; Bridgwater, A. V.; Gerhauser, H. Application of CFD to Model Fast Pyrolysis of Biomass. *Fuel Process. Technol.* **2009**, *90* (4), 504−512.
(27) Kaushal, P.; Abedi, J. A Simplified Model for Biomass Pyrolysis in a Fluidized Bed Reactor. *J. Ind. Eng. Chem.* **2010**, *16* (5), 748−755.
(28) Boateng, A. A.; Mtui, P. L. CFD Modeling of Space-Time Evolution of Fast Pyrolysis Products in a Bench-Scale Fluidized-Bed Reactor. *Appl. Therm. Eng.* **2012**, *33*−*34*, 190−198.
(29) Xue, Q.; Dalluge, D.; Heindel, T. J.; Fox, R. O.; Brown, R. C. Experimental Validation and CFD Modeling Study of Biomass Fast Pyrolysis in Fluidized-Bed Reactors. *Fuel* **2012**, *97*, 757−769.
(30) Xiong, Q.; Aramideh, S.; Kong, S.-C. Modeling Effects of Operating Conditions on Biomass Fast Pyrolysis in Bubbling Fluidized Bed Reactors. *Energy Fuels* **2013**, *27* (10), 5948−5956.
(31) Mellin, P.; Kantarelis, E.; Yang, W. Computational Fluid Dynamics Modeling of Biomass Fast Pyrolysis in a Fluidized Bed Reactor, Using a Comprehensive Chemistry Scheme. *Fuel* **2014**, *117*, 704−715.
(32) Boroson, M. L.; Howard, J. B.; Longwell, J. P.; Peters, W. A. Heterogeneous Cracking of Wood Pyrolysis Tars over Fresh Wood Char Surfaces. *Energy Fuels* **1989**, *3* (6), 735−740.
(33) Hoekstra, E.; Westerhof, R. J. M.; Brilman, W.; Van Swaaij, W. P. M.; Kersten, S. R. A.; Hogendoorn, K. J. A.; Windt, M. Heterogeneous and Homogeneous Reactions of Pyrolysis Vapors from Pine Wood. *AIChE J.* **2012**, *58* (9), 2830−2842.
(34) Li, D.; Briens, C.; Berruti, F. Improved Lignin Pyrolysis for Phenolics Production in a Bubbling Bed Reactor − Effect of Bed Materials. *Bioresour. Technol.* **2015**, *189*, 7−14.
(35) Du, C.; Liu, L.; Qiu, P. Importance of Volatile AAEM Species to Char Reactivity during Volatile−char Interactions. *RSC Adv.* **2017**, *7* (17), 10397−10406.
(36) Zhu, H.; Yi, B.; Hu, H.; Fan, Q.; Wang, H.; Yao, H. The Effects of Char and Potassium on the Fast Pyrolysis Behaviors of Biomass in an Infrared-Heating Condition. *Energy* **2021**, *214*, 119065.
(37) Dalluge, D. L.; Daugaard, T.; Johnston, P.; Kuzhiyil, N.; Wright, M. M.; Brown, R. C. Continuous Production of Sugars from Pyrolysis of Acid-Infused Lignocellulosic Biomass. *Green Chem.* **2014**, *16* (9), 4144−4155.
(38) Brown, R. C. Heterodoxy in Fast Pyrolysis of Biomass. *Energy Fuels* **2021**, *35* (2), 987−1010.
(39) Plouffe, C.; Peterson, C. A.; Rollag, S. A.; Brown, R. C. The Role of Biochar in the Degradation of Sugars during Fast Pyrolysis of Biomass. *J. Anal. Appl. Pyrolysis* **2022**, *161*, 105416.
(40) Huang, Y.; Liu, S.; Akhtar, M. A.; Li, B.; Zhou, J.; Zhang, S.; Zhang, H. Volatile−char Interactions during Biomass Pyrolysis: Understanding the Potential Origin of Char Activity. *Bioresour. Technol.* **2020**, *316*, 123938.
(41) Sun, Q.; Yu, S.; Wang, F.; Wang, J. Decomposition and Gasification of Pyrolysis Volatiles from Pine Wood through a Bed of Hot Char. *Fuel* **2011**, *90* (3), 1041−1048.
(42) Li, C.-Z. Importance of Volatile−char Interactions during the Pyrolysis and Gasification of Low-Rank Fuels − A Review. *Fuel* **2013**, *112*, 609−623.
(43) Scala, F.; Chirone, R.; Salatino, P. Combustion and Attrition of Biomass Chars in a Fluidized Bed. *Energy Fuels* **2006**, *20* (1), 91−102.
(44) Keown, D. M.; Hayashi, J.; Li, C.-Z. Effects of Volatile−char Interactions on the Volatilisation of Alkali and Alkaline Earth Metallic Species during the Pyrolysis of Biomass. *Fuel* **2008**, *87* (7), 1187−1194.
(45) Troiano, M.; Ianzito, V.; Solimene, R.; Ganda, E. T.; Salatino, P. Modelling Fast Pyrolysis of Biomass in a Fluidized Bed Reactor. *Can. J. Chem. Eng.* **2022**.
(46) Solimene, R.; Marzocchella, A.; Ragucci, R.; Salatino, P. Flow Structures and Gas-Mixing Induced by Bubble Bursting at the Surface of an Incipiently Gas-Fluidized Bed. *Ind. Eng. Chem. Res.* **2004**, *43* (18), 5738−5753.
(47) Santana, D.; Nauri, S.; Acosta, A.; García, N.; Macías-Machín, A. Initial Particle Velocity Spatial Distribution from 2-D Erupting Bubbles in Fluidized Beds. *Powder Technol.* **2005**, *150* (1), 1−8.

https://doi.org/10.1021/acs.energyfuels.2c01483
Energy Fuels 2022, 36, 9660−9671

(48) Almendros-Ibáñez, J. A.; Sánchez-Delgado, S.; Sobrino, C.; Santana, D. Experimental Observations on the Different Mechanisms for Solid Ejection in Gas-Fluidized Beds. *Chem. Eng. Process. Process Intensif.* **2009**, *48* (3), 734−744.
(49) Garcia-Gutierrez, L. M.; Soria-Verdugo, A.; Marugán-Cruz, C.; Ruiz-Rivas, U. Simulation and Experimental Study on the Motion of Non-Reacting Objects in the Freeboard of a Fluidized Bed. *Powder Technol.* **2014**, *263*, 112−120.
(50) Johnsson, F.; Leckner, B. Vertical Distribution of Solids in a CFB Furnace. *Proceedings of the 13th International Conference on Fluidized-Bed Combustion*; Orlando, FL, May 7−10, 1995; pp 671−679.
(51) Aronsson, J.; Lyngfelt, A.; Pallarès, D. Effects of the Choice of Gas on the Hydrodynamics of Fluidized Beds. *Ind. Eng. Chem. Res.* **2019**, *58* (20), 8847−8855.
(52) Djerf, T.; Pallarès, D.; Johnsson, F. Bottom-Bed Fluid Dynamics − Influence on Solids Entrainment. *Fuel Process. Technol.* **2018**, *173*, 112−118.
(53) Bruni, G.; Solimene, R.; Marzocchella, A.; Salatino, P.; Yates, J. G.; Lettieri, P.; Fiorentino, M. Self-Segregation of High-Volatile Fuel Particles during Devolatilization in a Fluidized Bed Reactor. *Powder Technol.* **2002**, *128* (1), 11−21.
(54) Iannello, S.; Foscolo, P. U.; Materazzi, M. Investigation of Single Particle Devolatilization in Fluidized Bed Reactors by X-Ray Imaging Techniques. *Chem. Eng. J.* **2022**, *431*, 133807.
(55) Köhler, A.; Pallarès, D.; Johnsson, F. Modeling Axial Mixing of Fuel Particles in the Dense Region of a Fluidized Bed. *Energy Fuels* **2020**, *34* (3), 3294−3304.
(56) Köhler, A.; Rasch, A.; Pallarès, D.; Johnsson, F. Experimental Characterization of Axial Fuel Mixing in Fluidized Beds by Magnetic Particle Tracking. *Powder Technol.* **2017**, *316*, 492−499.
(57) Douglas, J. M.; Bischoff, K. B. Variable Density Effects and Axial Dispersion in Chemical Reactors. *Ind. Eng. Chem. Process Des. Dev.* **1964**, *3* (2), 130−133.
(58) Shafizadeh, F.; Chin, P. P. S. Thermal Deterioration of Wood. In *Wood Technology: Chemical Aspects*; Goldstein, I. S., Ed.; American Chemical Society (ACS): Washington, D.C., 1977; ACS Symposium Series, Vol. *43*, Chapter 5, pp 57−81, DOI: 10.1021/bk-1977-0043.ch005.
(59) Di Blasi, C.; Branca, C. Kinetics of Primary Product Formation from Wood Pyrolysis. *Ind. Eng. Chem. Res.* **2001**, *40* (23), 5547−5556.
(60) Liden, A. G.; Berruti, F.; Scott, D. S. A Kinetic Model for the Production of Liquids from the Flash Pyrolysis of Biomass. *Chem. Eng. Commun.* **1988**, *65* (1), 207−221.
(61) Di Blasi, C. Analysis of Convection and Secondary Reaction Effects Within Porous Solid Fuels Undergoing Pyrolysis. *Combust. Sci. Technol.* **1993**, *90* (5−6), 315−340.
(62) Shi, X.; Ronsse, F.; Pieters, J. G. Finite Element Modeling of Intraparticle Heterogeneous Tar Conversion during Pyrolysis of Woody Biomass Particles. *Fuel Process. Technol.* **2016**, *148*, 302−316.
(63) Sadhukhan, A. K.; Gupta, P.; Saha, R. K. Modelling of Pyrolysis of Large Wood Particles. *Bioresour. Technol.* **2009**, *100* (12), 3134−3139.
(64) Pattanotai, T.; Watanabe, H.; Okazaki, K. Experimental Investigation of Intraparticle Secondary Reactions of Tar during Wood Pyrolysis. *Fuel* **2013**, *104*, 468−475.
(65) Shen, Y. Chars as Carbonaceous Adsorbents/Catalysts for Tar Elimination during Biomass Pyrolysis or Gasification. *Renewable Sustainable Energy Rev.* **2015**, *43*, 281−295.
(66) Ravenni, G.; Sárossy, Z.; Ahrenfeldt, J.; Henriksen, U. B. Activity of Chars and Activated Carbons for Removal and Decomposition of Tar Model Compounds − A Review. *Renewable Sustainable Energy Rev.* **2018**, *94*, 1044−1056.
(67) Cheng, L.; Wu, Z.; Zhang, Z.; Guo, C.; Ellis, N.; Bi, X.; Paul Watkinson, A.; Grace, J. R. Tar Elimination from Biomass Gasification Syngas with Bauxite Residue Derived Catalysts and Gasification Char. *Appl. Energy* **2020**, *258*, 114088.
(68) Hosokai, S.; Kumabe, K.; Ohshita, M.; Norinaga, K.; Li, C.-Z.; Hayashi, J. Mechanism of Decomposition of Aromatics over Charcoal and Necessary Condition for Maintaining Its Activity. *Fuel* **2008**, *87* (13), 2914−2922.
(69) Abu El-Rub, Z.; Bramer, E. A.; Brem, G. Experimental Comparison of Biomass Chars with Other Catalysts for Tar Reduction. *Fuel* **2008**, *87* (10), 2243−2252.
(70) Fuentes-Cano, D.; Gómez-Barea, A.; Nilsson, S.; Ollero, P. Decomposition Kinetics of Model Tar Compounds over Chars with Different Internal Structure to Model Hot Tar Removal in Biomass Gasification. *Chem. Eng. J.* **2013**, *228*, 1223−1233.
(71) Geldart, D.; Cullinan, J.; Georghiades, S.; Gilvray, D.; Pope, D. J. Effect of Fines on Entrainment from Gas Fluidised Beds. *Trans. Inst. Chem. Eng.* **1979**, *57* (4), 269−275.
(72) Tasirin, S. M.; Geldart, D. Entrainment of FCC from Fluidized Beds — A New Correlation for the Elutriation Rate Constants Ki∞*. *Powder Technol.* **1998**, *95* (3), 240−247.
(73) Wen, C. Y.; Yu, Y. H. A Generalized Method for Predicting the Minimum Fluidization Velocity. *AIChE J.* **1966**, *12* (3), 610−612.
(74) Haider, A.; Levenspiel, O. Drag Coefficient and Terminal Velocity of Spherical and Nonspherical Particles. *Powder Technol.* **1989**, *58* (1), 63−70.
(75) Cho, H. Il; Chung, C.-H.; Han, G. Y.; Ahn, G. R.; Kong, J. S. Axial Gas Dispersion in a Fluidized Bed of Polyethylene Particles. *Korean J. Chem. Eng.* **2000**, *17* (3), 292−298.
(76) Sternéus, J.; Johnsson, F.; Leckner, B. Gas Mixing in Circulating Fluidised-Bed Risers. *Chem. Eng. Sci.* **2000**, *55* (1), 129−148.
(77) Solimene, R.; Marzocchella, A.; Ragucci, R.; Salatino, P. Laser Diagnostics of Hydrodynamics and Gas-Mixing Induced by Bubble Bursting at the Surface of Gas-Fluidized Beds. *Chem. Eng. Sci.* **2007**, *62* (1), 94−108.
(78) Tebianian, S.; Solimene, R.; Salatino, P. Flow Structures and Mixing Patterns in the Freeboard of Gas-Fluidized Bed Reactors. *Ind. Eng. Chem. Res.* **2014**, *53* (22), 9296−9302.